PHYSICAL REVIEW B VOLUME 14, NUMBER 2 15 JULY 1976

Field-emission energy spectroscopy of the platinum-group metals*

N. J. Dionne† and T. N. Rhodin‡
School of Applied and Engineering Physics, Cornell University, Ithaca, New York 14853
(Received 17 November 1975)

Energy-distribution functions have been measured for field-emission electron currents from the (100), (110), (210), (211), and (311) faces of field-evaporated rhodium, iridium, and platinum emitters and from the (100) and (111) faces of a field-evaporated palladium emitter. The structures contained in these energy spectra are interpreted in terms of current contributions among overlapping sub-bands of calculated, electronic band structure for the bulk metal. A systematic correlation between the calculated band-edge eigenvalues and the details of the energy spectra is observed. It is concluded that the field-emission spectra for the platinum-group metals contain many of the directional features of the electronic band structure for the bulk material. General predominance of t_{2g} bands relative to the Γ-centered bands characterizes the normalized field-emission spectra, which are believed to contain directional, local density-of-states information. Adsorption of saturation layers of hydrogen and nitrogen on the (100), (110), (210), and (111) faces of rhodium indicate suppression of the e_g bands relative to the t_{2g} bands for states in the surface-normal direction. Implications with reference to the specific electron structure of the surfaces of platinum-group metals and the effects of chemisorption on the surface electron structure are discussed.

I. INTRODUCTION

It is now apparent from the work of Penn and Plummer[1] and from Politzer and Cutler[2] that the local density of states, strongly weighted in the surface-normal direction, is uniquely extractible from experimental field-emission-energy-distribution (FEED) data. This "directionality" feature distinguishes field-emission spectroscopy from other surface spectrographic techniques as ion-neutralization spectroscopy, ultraviolet-photoemission spectroscopy etc., which rely upon electronic transitions involving a nondirectional joint density of states.[3-5] Because the tunneling process samples approximately the electronic probability density function at the classical turning points,[1] FEED spectroscopy is an effective probe[6,7] of the electronic band structure at the immediate metallic surface within a few eV spread near the Fermi level. It should be noted that only very careful deductions can be made with reference to deducing the local density of states or the character of the wave functions at the surface. The associated limitations particularly for tunneling spectra from the high index planes is discussed in some detail in Sec. V.

In a previous letter,[8] we have indicated the suitability of the fcc platinum-group metals for electronic band-structure studies by means of FEED spectroscopy. According to recent relativistic augmented-plane-wave band-structure calculations,[9] the subband locations of the strongly hybridized d bands for these transition metals occur in the vicinity of the Fermi level. Hence, the potential for a systematic study of d bands via FEED spectroscopy is particularly favorable for the case of the platinum-group metals. In this paper we present the normalized field-emission spectra for the clean, principal planes of all four (fcc) platinum-group metals; rhodium, palladium, iridium and platinum. With the availability of a consistent set of calculated electronic band structure, we are able to interpret many of the salient structural details contained in these FEED spectra and to perform spectral decompositions in terms of the relative contributions among overlapping subbands. The platinum-group metals are well known for their catalytic properties such as the hydrogenolysis and hydrogenation of organic compounds.

Attempts to understand these properties by a variety of experimental methods, including surface spectrographic techniques, are currently underway. When examined from a subband point of view, it is possible to gain further insight into these processes by observing the effects of gaseous adsorption upon the structural content of FEED spectra. In this regard, we provide an illustration of this approach by using the results of hydrogen and nitrogen adsorption on selected planes of rhodium. Not surprisingly, the crystallographic dependence of these structural changes is seen to be specific to the adsorbate and to the subbands.

Comparisons of experimental FEED studies on copper,[10] tungsten, and molybdenum[6,11] with calculated, bulk band structure have been seriously limited because of uncertainties both in the interpretation of the spectra and in the reliability of the band-structure calculations. More recent studies on nickel[12] using an energy analyzer of limited sensitivity failed to reveal indications of the d

bands. Field-emission calculations resulting from a variety of models[2,7,13-17] have indicated the predominance of the s-p bands in the general shape of the experimental FEED curves. Spectral contributions of the d-bands (in the tight-binding approximation) have been expected to be comparatively slight—as much as a factor of 100 smaller.[2,6,7,15-17] However, in the case of the strongly hybridized d bands of the platinum-group metals, the relative contributions of the overlapping subbands to FEED spectra should reflect the strong admixture of atomic s-p and d states. In terms of the d-electron count, the fcc platinum-group metals provide a natural sequence in which to investigate the relative d character of the subbands from a consistent point of view. Perhaps, more important is the possibility for extracting the subband eigenvalues from the FEED spectra for these materials.

Interpretation of experimental FEED spectra in terms of subband effects requires at least a qualitative appreciation for the approximate spectral shapes which individual subband contributions at the metallic surface might assume. To this end the availability of reliable band-structure calculations is an indispensable advantage. Formal calculations of FEED spectra along the lines of Politzer and Cutler[2] on nickel and more recently by Nicolau and Modinos on tungsten,[17] which include Block waves and individual d-band energy-surface contours, represent substantial progress toward quantitative comparisons with experimental FEED spectra. In the absence of similar computations for the platinum-group metals, it is nonetheless possible to utilize the insights derived from calculated bulk band structures in order to deduce the subband contributions to FEED spectra.

Our plan for this paper begins with our experimental approach to FEED measurement in Sec. II. An energy analyzer of novel design is described in some detail. Theoretical considerations are developed heuristically (rather than in specially assigned sections). Section III summarizes the normalized FEED spectra for the platinum-group metals. In Sec. IV, we interpret these spectra and perform selected spectral decompositions. Finally, the manifestations of the directional, local density of states, associated with individual subbands, are examined in Sec. V; and the effects of gaseous adsorption (hydrogen and nitrogen) upon the normalized spectra for the low-index planes of rhodium are indicated.

II. EXPERIMENTAL FEED MEASUREMENT

In this section, we outline the basic experimental approach used to obtain results summarized and discussed in the following sections. First, a description of the field-emission-microscope–energy-analyzer system is made. Second, the method for data acquisition and reduction is detailed. Third, preparation techniques for the emitter materials are indicated. Finally, theoretical considerations regarding the experimental FEED spectra are then developed to clarify the underlying nature of the FEED measurement.

The field emission microscope, invented by Müller, permits a great variety of ingenious modifications. Typically, one places an electrochemically etched tip of very small radius (of order 1000 Å) inside an anode deflection system, all of which are maintained at low temperature within an ultrahigh-vacuum chamber (10^{-11}–10^{-10} Torr). Application of a high electric field (a few tenths of a volt per angstrom) provides sufficient barrier-penetration current to image the general, crystallographic features of the emitter tip onto a phosphor-coated screen. Because of the conservation of angular momentum, the observed field-emission, intensity pattern reflects the local field and work function changes along the tip surface. Incorporation of an electrostatic anode-deflection system permits current from local regions of the emitter surface to pass through a probe hole for the purpose of total energy analysis. By this technique, the experimentalist is able to monitor local current variations as well as total current changes with the emitter potential. Consequently, it is possible to extract a crystallographically dependent, local work function.[18] Since several crystallographic planes can be developed simultaneously on a field emission tip, many crystallographic faces are conveniently assessible for investigation on the same experimental crystal surface.

In practice, considerable complexity is introduced into the basic FEED measurement system in order to facilitate precise measurements of emission spectra under a wide variety of experimental conditions. Since single adsorption events can seriously alter localized surface tunneling properties, the time interval during which clean surface conditions prevail is critically dependent upon attainment of ultrahigh vacuum levels. Field-emission materials exhibit finite limits on the current densities which can be obtained stably prior to thermal breakdown, thermal diffusion, or desorption of chemisorbed gases under study. In view of the strong exponential dependence which characterizes field-emission spectra, it becomes essential to design instrumentation which can detect very small currents sensitively over a wide dynamic range. Typically, the combined effects of the above factors limit statistically significant

FEED measurements to an energy range of a few eV below the Fermi level.

Central to the FEED measurement is the performance of an energy analyzer. Basically, high-energy resolution, fast instrument response time, high current sensitivity, efficient detection, low noise, and linear optics include most of the important considerations which must be contemplated in the design of the instrumentation. Unfortunately, there are only too few practical designs which have been developed to meet these needs. Plummer[7] has reviewed some instruments currently in use. Of these designs, at present, only those employing spherical deflection systems have approached desirable performance levels, but at prohibitive cost for small laboratory use.

We have developed an electron energy analyzing system incorporating an energy analyzer of novel design.[19] Its performance compares favorably with existing high performance spherical systems (dynamic range of six orders of magnitude, operating voltage range 400–3000 V, and an energy resolution of 15 to 70 meV). Its primary advantage is gained through its compact cylindrical design which lends itself to economical, uncomplicated fabrication and assembly. Pictured in Fig. 1, the grid-cell energy analyzer is composed of three sections. The electron beam from a local region on the emitter emerges from the probe hole into a deceleration lens system of four electrodes in region I. To avoid excessive spherical and chromatic aberrations, the voltage ratios of these electrodes are adjusted to provide two axial crossings for which the first focal length is large compared with the second. By placing the image plane (at the second crossing) at a short distance from the second focal plane, we are able to obtain tenfold angular magnification. Given a prescribed angular magnification and kinetic energy reduction, the diverging beam then continues through a double-pass grid-cell system (region II) only if the electron kinetic energy lies within a narrow energy-band pass. Characterized by low spherical aberration, but high chromatic aberration, this dual grid-cell lens[19] is composed of three apertured electrodes (4, 6, and 8) of the same electrostatic potential and two electrodes (5 and 7) each housing thin molybdenum foils on which a fine mesh is photoetched in an annular region concentric with the optical axis. By adjusting the potential of each annular grid in a manner which will retard electrons to velocities corresponding to several meV, we are able to achieve an energy band pass of 15–75 meV. Electrons not having sufficient kinetic energy are reflected from the grid region to the aperture walls, and electrons having excessive kinetic energies are not able to pass through all three apertures because of the strong chromatic aberration attending off-axial trajectories. Finally, the energy-analyzed beam

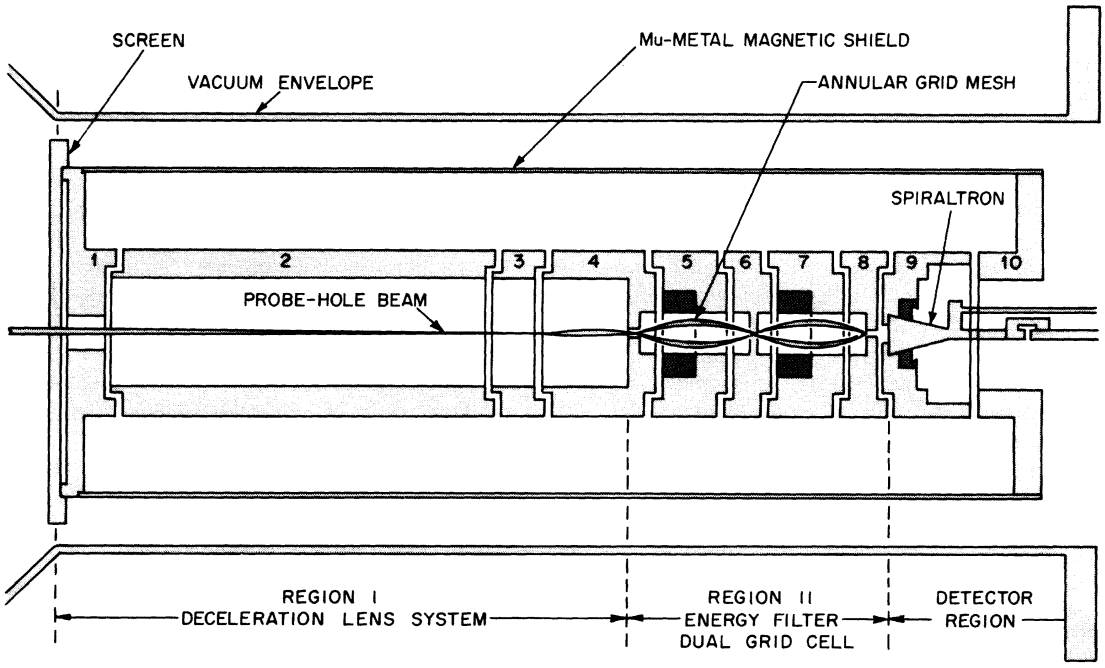

FIG. 1. Grid-cell energy analyzer.

enters the electron multiplier (region III) for single electron detection via pulse counting techniques. An energy spectrum is obtained by sweeping the common level of the electrode potentials and storing the detected electron counts in a computerized data acquisition system, represented in Fig. 2.

After the spectral data have been acquired for a freshly field-evaporated emitter (at liquid-nitrogen temperature) and corrected for systematic errors, we then calculate normalized spectra based upon the standard FEED expression,[7] $J'(\epsilon)$, which has been corrected for the energy-analyzer resolution error:

$$J'_{0c}(\epsilon) = \int_{-\infty}^{\infty} J'(\epsilon)\, G(\epsilon, \epsilon')\, d\epsilon' \ . \tag{1}$$

We have assumed the form of the instrument error to be described by the normal distribution[20]

$$G(\epsilon, \epsilon') = \exp\{-[(\epsilon - \epsilon')/\sqrt{2}\sigma]^2\}/\sigma\sqrt{2\pi}\ , \tag{2}$$

where the full-width-at-half-maximum points are separated by 2.36σ, the resolution width. For reasons which will be made clear, we have normalized the experimental curves by using the standard FEED current[7] form

$$J'(\epsilon) = Ae^{\epsilon/d} f(\epsilon), \tag{3}$$

where ϵ is the normalized energy with respect to the Fermi level; $f(\epsilon)$, the Fermi function; and d, an energy parameter. Determination of d, A, σ are obtained by judicious curve fitting to appropriate pieces of the experimental curves and by utilizing insights gained from calculated band structure. The primary reasons for obtaining a normalized field-emission spectral function

$$R'(\epsilon) \equiv J'_{\text{exp}}(\epsilon)/J'_{0c}(\epsilon) \tag{4}$$

are to remove the strong exponential shape of the experimental curve $J'_{\text{exp}}(\epsilon)$, and to minimize the contributions of temperature, field, and instrumental error to the distortions inherent in the general form of the experimental curves.

Field evaporation of the emitter surfaces prior to a data run is essential to ensure cleanliness of the surfaces and also to develop individual planes into large nonequilibrium sizes in order to minimize uncertainties resulting from planar edge-site current. Field-emission imaging following each transient evaporation is adequate to monitor individual planar-size evolution for several low-index planes of the platinum-group metals.

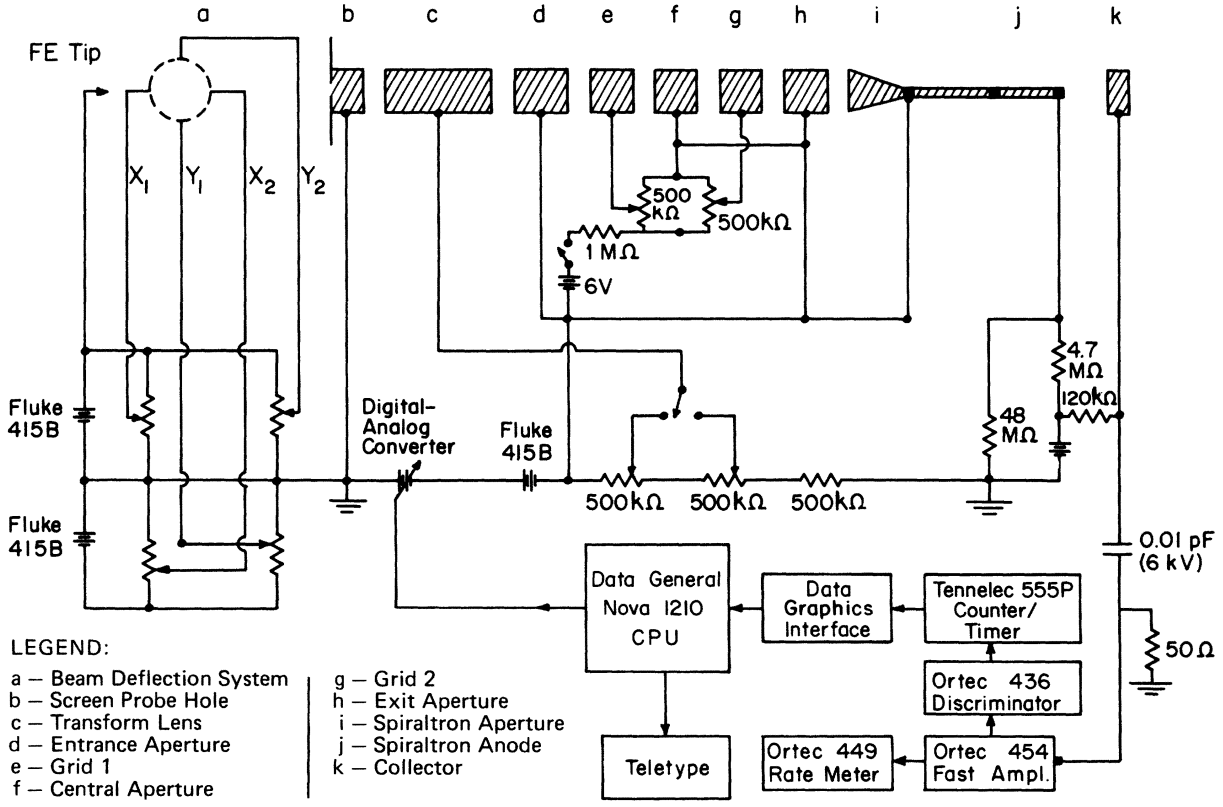

FIG. 2. FEED data acquisition system—electrical layout.

Electrochemical etching of the materials (~99.99+% pure) was performed by the direct-emersion method. For iridium, a 1*N* solution of NaOH at 4.5 V ac provided adequate pre-etching. However, subsequent reduction to a 0.2 *N* solution, use of a capillary, and a voltage setting of 6.5 V ac produced best results. Rhodium, palladium and platinum, on the other hand, etched readily in a molten salt bath of NaCl(15%) and $NaNO_3$(85%) using 3.5–4.5 V dc. At 4.5 V dc, palladium sharpened better in a nitric acid solution (three parts water).

In general, we consider the FEED measurement to involve the total energy distribution of field-emission current, weighted over an extended region of the emitter surface. The detected current is derived from the neighborhood of a geometrically determined annulus at the tip's surface.

The uncertainty principle, beam broadening, edge-site atoms, asperities, defects, and adsorbates can give rise to current originating outside the annular zone. For this reason, large planar regions are essential for one-dimensional probing of the surface electronic band structure. Otherwise, scattering of electronic states having substantial transverse crystal-momentum may significantly influence the value of the surface-averaged current.

III. NORMALIZED FEED SPECTRA OF THE PLATINUM-GROUP METALS

Discussion concerning the structural details contained in experimental field-emission spectra is aided greatly by reference to their associated normalized FEED spectra in which the general exponential shape is removed in some appropriate way. Certain aspects of their construction, discussed in the previous section, require a qualitative understanding of both the emission process and the electronic band structure of the emitter. Therefore, theoretical considerations of the energy distribution function for the field-emission current will be treated in anticipation of the normalized spectra of the platinum-group metals presented later in this section.

In a real metallic crystal the electronic states are described by infinite sets of Bloch waves[20] which form standing waves because of the presence of the surface barriers. Specifically, we may choose the single-particle band picture in which the electronic states are solutions of the one-electron Schrödinger equation for the nth band,

$$[-\hbar^2\nabla^2/2m + V(\vec{r}) + \Sigma]\psi_{n,\vec{k}}(\vec{r}) = E_n\psi_{n,\vec{k}}(\vec{r}) , \quad (5)$$

where Σ is a complicated exchange and correlation operator and $V(\vec{r})$ is a periodic lattice potential except in the surface region. The requirement that the wave functions and their derivatives be finite, single-valued, and continuous everywhere results in exponentially decaying tails outside the metallic surface. The Bloch states for metallic crystals of finite size can also be included in solutions involving band gaps where standing waves are exponentially damped inwardly from the surface, in which case the wave vector $\vec{k}$ is complex. For our purposes, the important consideration is that the standing-wave amplitudes be spatially varying in the surface region. Since this positional dependence is expected to influence the field-emission energy spectra, we discuss the concept, termed "the local density of states." As defined by Friedel,[21] the local density of states at some position $\vec{r}$ is given by

$$n(\epsilon, \vec{r}) = \sum_m \psi_m^*(\vec{r})\,\psi_m(\vec{r})\,\delta(\epsilon - \epsilon_m) , \quad (6)$$

where the probability density is summed upon all metallic states m at energy ϵ. Summation upon the δ function gives the usual spatially independent density of states. Thus, the local density of states expresses the probability per unit volume per unit energy of finding an electron at energy ϵ and at point r. Application of this concept to d bands of transition metals has indicated crystallographic variations in the degree of energy-band compressions.[22,23]

One of the potential applications of FEED concerns the possible detection of these surface band-structural features in terms of the local density of states. Penn and Plummer[1] have reconsidered the field-emission problem from the transfer Hamiltonian point of view in the WKB approximation. Using a one-dimensional model, they show how the local density of states can manifest itself in an approximate fashion in FEED curves. Given that the surface potential barrier is planar, the transmitted electron is assumed to be a "bare" electron with a well-defined transverse momentum which can be related to an approximate (WKB) wave function at the classical turning point. The result of their analysis takes the form

$$J'(\epsilon) \cong Cf(\epsilon) \sum_m D(W_m)(\psi_m^*\psi_m)_{tp}\,\delta(\epsilon - \epsilon_m) , \quad (7)$$

in which the factor C has slowly varying dependence upon energy. For typical field-emission operating conditions, the tunneling probability function $D(W_m)$ is presumed[24,25] to have a strong exponential dependence upon the transverse component of crystal momentum at the surface barrier through the "normal" component of energy,

$$W_m = \epsilon_m - \hbar^2 k_{t,m}^2/2m \ . \tag{8}$$

Consequently, only metallic states with small values of $k_{t,m}$ are expected to have appreciable contribution to the current distribution function. However, Politzer and Cutler[2] have shown that this deduction is not generally true for d-bands in real metals for reasons having to do with the directionality of the atomic orbitals in the Bloch function. Comparing the current distribution function of Eq. (7) with the local density-of-states function of Eq. (6) leads to the conclusion that FEED measurements can sample approximately the local density of states, exponentially weighted in the surface-normal direction *at* the classical turning points. It is this "directionality" aspect of the measurements which gives rise to the advantage of FEED surface spectroscopy over other spectroscopic surface-sensitive techniques.

Application of Eq. (7) to real metals should not be done without consideration of some additional factors. First, the three-dimensional nature of the surface barrier may result in spatial variations of $|\psi_m|^2$ and $D(W_m)$ along the surface to an extent which can pose conceptual difficulties.[2] The WKB wave function precludes the two-dimensional Bloch formulation of FEED theory.[2,17] Therefore, we must be content to use the surface-averaged results for these quantities. Second, the location and shape of the interior surface locus of classical turning points are not independent of the electron state or electron band. The one-electron potential barrier can have different shapes and thickness depending upon the type of atomic orbitals involved in the Block states. For example, d bands might be expected to have classical turning points occurring closer to the interior of the metal, relative to the s-p bands. Third, the assumption of specular reflection does not allow the possibility for surface scattering into the direction normal to the surface atomic layer from metallic states having values of $k_{t,m}$ close to the reciprocal lattice vectors of the surface plane. Finally, the tunneling probability function $D(W_m)$ may not be adequately described in the WKB approximation.[26,27] Nevertheless, on large close-packed planes of an emitter, the Penn-Plummer expression for FEED current appears to be a useful approximation.

Application of Eq. (7) to a Sommerfeld metal leads to an expression equivalent to the standard FEED equation originally developed by Young[28] for a free-electron metal using an image potential barrier

$$J_f'(\epsilon) = J_0 e^{\epsilon/d} f(\epsilon)/d \ , \tag{9}$$

in which J_0 is the Fowler-Nordheim current and d is an energy parameter relating to the work function and applied field. Since Eq. (9) describes the general shape of the FEED curves, it is convenient to express FEED current for a real metal in terms of Young's[28] result; or

$$J'(\epsilon) = (J_0/d)\, e^{\epsilon/d} f(\epsilon) R'(\epsilon) \ , \tag{10}$$

where

$$R'(\epsilon) = \sum_j \frac{n(\epsilon, k_\perp^j)}{n_f(\epsilon)} \tag{11}$$

is the normalized spectra summed over the overlapping bands. Here, $n(\epsilon, k_\perp^j)$ is the weighted local density of states [see the summation in Eq. (7)] in the $k_\perp^j$ direction for the jth subband; and $n_f(\epsilon)$ is the weighted local density of states for a free-electron metal.

Experimentally, the resolution error of the energy analyzing system alters the FEED spectra represented by Eqs. (10) and (11). Thus, we have elected to use an experimental, normalized FEED spectra in which the measured current distribution function, $J_m'(\epsilon)$, is normalized with respect to that for a free-electron metal, corrected for resolution broadening according to

$$R_m'(\epsilon) = J_m'(\epsilon) \left(\int_{-\infty}^{\infty} J_f'(\epsilon')\, G(\epsilon, \epsilon')\, d\epsilon' \right)^{-1} . \tag{12}$$

The normal distribution function $G(\epsilon, \epsilon')$ is given in Eq. (2). Spectral data normalized in the above manner, can thus be examined conveniently since effective removal of the Fermi-function factor, its distortion by the instrument error, and the exponential shapes with their field dependencies are approximately achieved. For high-resolution FEED measurement systems, the experimental normalized spectra of Eq. (12) should reflect the normalized, directional local density of states expressed by Eq. (11).

Application of Eqs. (9)—(12) to experimental FEED spectra, containing pronounced structural details as in the case of the platinum-group metals, can be somewhat uncertain unless the data extend over an energy range sufficient to establish the slope of the overriding s-p character of the experimental curves through the energy parameter d. For the platinum-group metals, we can resolve this problem upon consideration of the systematic electronic band-structure calculations performed by Andersen,[9] using the *a priori* relativistic augmented-plane-wave method. Andersen's computational results for this grouping are reproduced in Fig. 3 for the principal symmetry points. Depending upon the crystallographic direction and energy level, we observe that field-emission current might originate from as many as

four overlapping subbands over the energy range assessible for FEED measurement (within ~2.0 eV of E_F). Of particular interest are the edge locations of the various d bands within the measurable energy range. The bands spanned by the lower and upper Γ_{8+} points are identified as the d bands and are numbered in the order of increasing energy near the degenerate Γ points. For instance, the Γ-centered bands of the e_g group (denoted by the upper Γ_{8+} point) occur in the convenient range of -1.4 to -0.9 eV for all four platinum-group metals. In the special case of the close-packed planes on iridium and platinum, we can expect to locate the upper bound for the third d band (one of the three t_{2g}-group bands).

Since our objective is to construct normalized FEED spectra in order to make meaningful comparisons with band-structure curves (Fig. 3), we focus our attention upon the energy region below the Γ-centered bands ($\epsilon < -1.4$ to -0.9 eV). Assuming we can identify a portion of the experimental FEED spectrum which is consistently structureless [$\log_{10}(-J)$ varies linearly with ϵ], we are able to ascribe a free-electron-like character to this region. Apparently, all of our experimental FEED curves[19] for the platinum-group metals, without exception, have been observed to have an approximately linear nature in this low-energy range for the principal, crystallographic planes and directions investigated. Hence this constitutes a strong base for this assumption. According to the dispersion curves of Fig. 3, this energy zone excludes all but the overlapping second and third d bands. However, from the broad shapes of these curves, it is apparent that they are somewhat s-p-like[9] within these midband zones and, therefore, are expected to provide structureless, classical FEED spectra. Hence, construction of the normalized FEED spectra of Fig. 4 is based upon fitting the corrected, standard FEED expressions of Eqs.

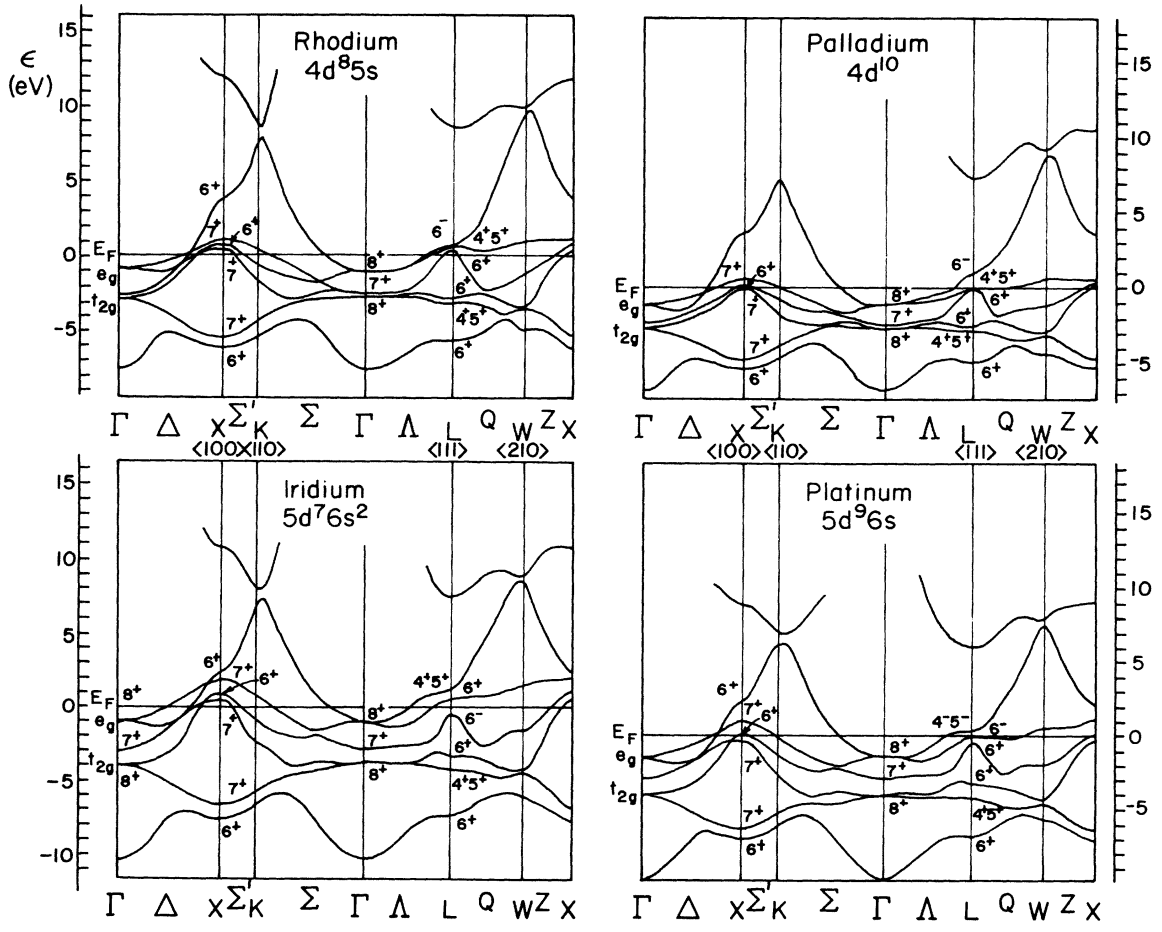

FIG. 3. Calculated (relativistic augmented-plane-wave band structure of the platinum-group metals [Andersen (Ref. 9)]. For convenience, the principal directions are labeled with Miller indices.

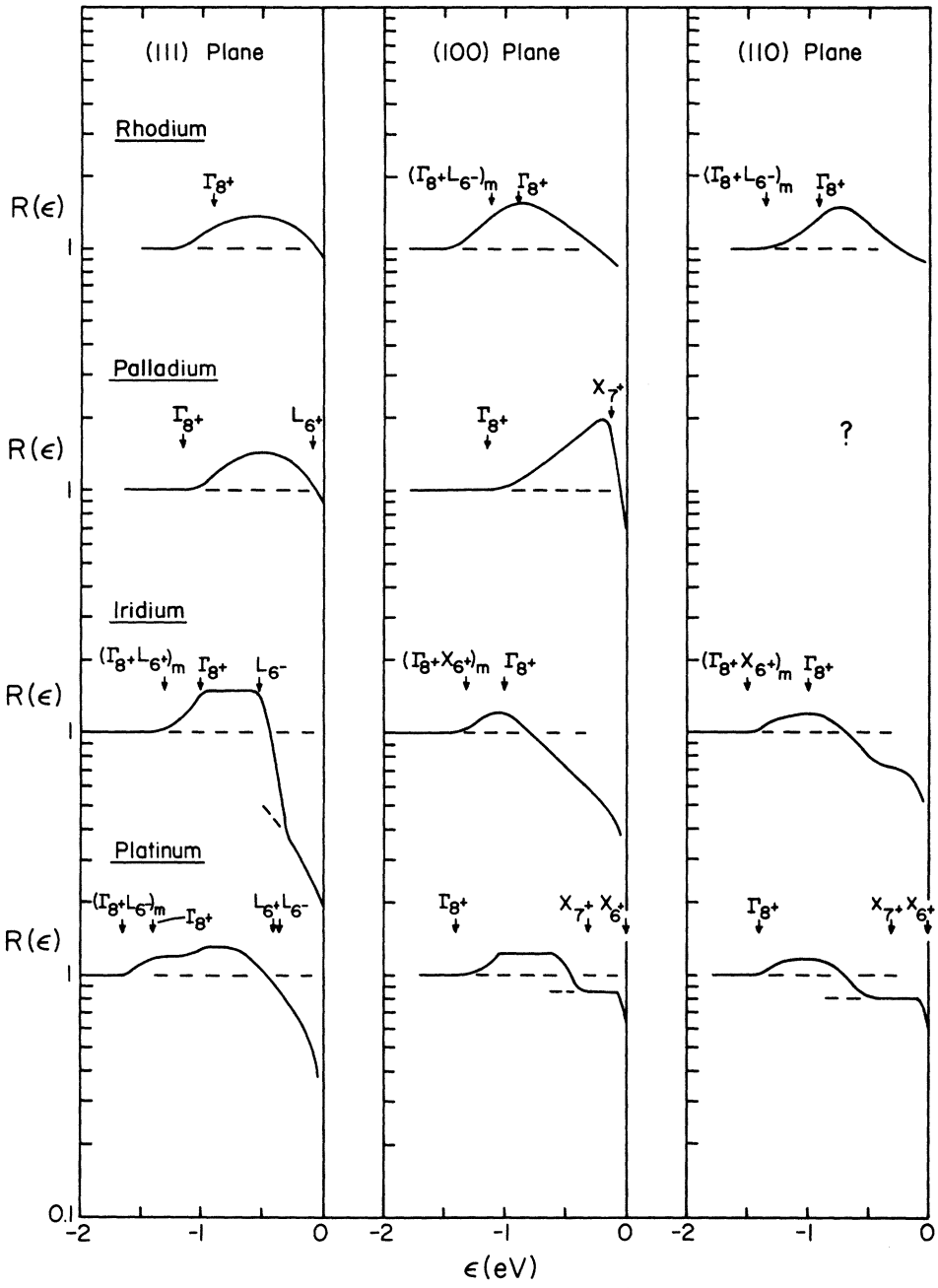

FIG. 4. Enhancement factors for the clean low-index planes of the platinum-group metals. Arrows indicate locations of the appropriate band-edge extremes from calculated energy-band structure.

(9)–(12) to this portion of the experimental curves. Since the energy bands overlap the Fermi level, the location of the latter ($\epsilon_F = 0$) in the normalized spectra is estimated to be accurate within ±0.05 eV.

In Fig. 4, we provide a collection of the experimental, normalized FEED spectra for each of the principal planes for all four metals of the fcc platinum group with the exception of Pd(110), which has not yet been obtained. Locations of various energy eigenvalues associated with the subband extrema[9] are inserted for comparisons with the structural details. It is significant that all of the lower-energy boundaries for the structural prominences fall within 0.1 eV of the calculated minimum values of the Γ-centered bands (denoted by the upper Γ_{8^+} point or by the double-letter notation). Exception to this rule is noted for Rh(100) and Rh(110) because the bottom of the fourth *d* band is estimated to be 0.3 eV higher than the observed points of onset for the structural prominences. In making these comparisons, it is important to con-

sider our assumptions regarding the directional character of the tunneling process and the s-p–like behavior of the second and third d bands in their midband regions below the upper Γ_{8^+} point. Justifications for these are implicit in the discussions of the following sections in which the significance of these apparent correlations is considered.

IV. SPECTRAL DECOMPOSITION OF OVERLAPPING d-BANDS

Several features of the normalized FEED spectra of Fig. 4 require comment. The spectral shapes fall into two groupings. In the first instance, we observe rounded symmetrically formed "mounds" (exemplified by rhodium) superposed on an otherwise structureless curve. The widths of these mounds have an approximate value of 1 eV. In the second grouping, represented by iridium and platinum data, these prominences are characterized by strongly descending slopes near the Fermi level. A third aspect of these structures, as in the case of Pt(100), Pt(110), and Ir(111), is the phenomenon of two or more parallel line segments. Finally, there is an apparent narrowing or compression of the mounds associated with the (110) planes relative to those of the (100) planes on both rhodium and platinum. Although it is presently difficult to provide detailed explanation for these effects, the band-structure curves of Fig. 3 are found to be a helpful guide in the interpretation of these generalized structural features. Not only is it possible to identify these structures with the overlapping subband current contributions but in some instances, reasonable arguments can be made for the decomposition of these spectral curves into constituent subband contributions. In the following discussion, we consider examples of these decompositions, various features of the local density of states, and finally the "directionality" inherent in the spectral structure.

Evaluation of the band-structure contributions in the normalized FEED spectra is complicated by several competing processes. First, we do not know the exact shape each subband current contribution would take. We have already noted that the free-electron-like segments of the subband dispersion curves would provide structureless current contributions. However, where d-like character of the subband segments predominate, we must proceed with caution. Near the band edges where the group velocity approaches zero, the density of states is highest in the bulk material. On the other hand, because of the way in which the s-p bands hybridize with the d bands, these band segments are often more d-like in nature. Thus, the wave functions would be spatially more confined to the surface atoms; consequently, the high density of states might be largely countered by a substantially reduced probability density at the classical turning points. Other contributing factors having to do with band-edge compression, energy surface topology, and the bonding and antibonding character of the electronic states at the surface combine to modify the form of the current contributions for the individual subbands. Although a directional local density of states can be calculated[22,23] and deduced from band-structure curves, construction of a directional local density of states at the metallic surface is not achievable with any accuracy. This is because detailed information regarding the wave functions for these strongly hybridized states is not generally available nor is it specifically known at the classical turning points. Calculations of d-band contributions for nickel[2] and tungsten[7,17] represent an important initial step toward rectification of this problem. Nonetheless, we can trace some qualitative features which can be anticipated in the forms of normalized spectra for subbands of various characterizations.

For the free-electron-like subband, the normalized FEED spectra according to Eqs. (9)–(12) should be rectangular in shape as depicted in Fig. 5(a). If all overlapping subbands had s-p–like character, then normalized FEED spectra would be marked with steps interconnected by straight-line segments as suggested in the curves for Pt(100) and Pt(110) in Fig. 4. Actually, we can expect rounding of the band edges for free-electron-like bands for energy surface topological reasons.[24,25] Stratton[25] has shown that the current distribution function depends only upon the cross section of the constant energy surface in the direction of emission but not upon the details of the surface topology. In this extension of Young's development, the standard equation (9) is modified by the so-called band-structure term (assuming conservation of transverse momentum). The resulting normalized spectrum is expressed by

$$R'(\epsilon) = 1 - \frac{1}{2\pi}\int_0^{2\pi} e^{-E_t(\epsilon,\phi)/d}\, d\phi \,, \tag{13}$$

where $E_t(\epsilon, \phi)$ is the kinetic energy associated with the extreme transverse component of crystal momentum traced along the perimeter of the projected constant energy surface onto the transverse plane in k space. For small values of $E_t(\epsilon, \phi)$ relative to the energy parameter d (typically $d \cong 0.1$ to 0.3 eV), $R'(\epsilon)$ is diminished by the second term in Eq. (13). This effect is illustrated by the occurrence of band-edge compression in Fig. 5(a).

Viewing the d bands as resonant bands in the tight-binding approximation, one might expect the

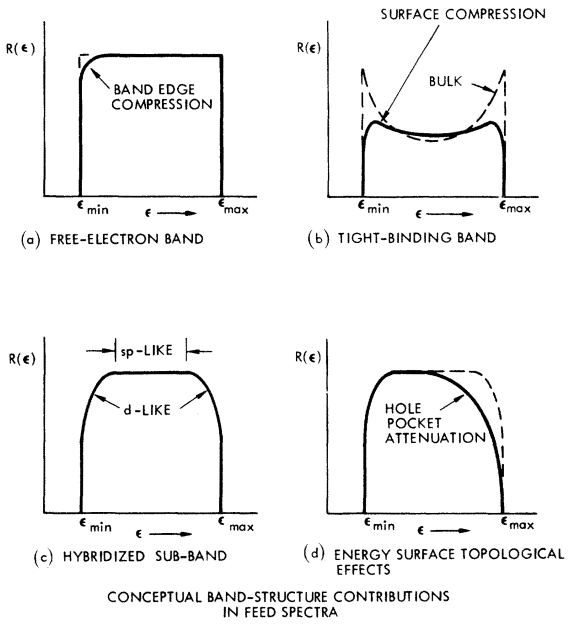

FIG. 5. Conceptual band-structure contributions in FEED spectra.

normalized FEED spectrum to be peaked at the band edges as indicated by the dashed curve in Fig. 5(b). In the bulk, the local density of states near the regions of small group velocity is generally a maximum. However, near the metallic surface, the local density of states differs from its shape[2,19,22–24] in the bulk for reasons having to do with the surface barrier and the reduced coordination number for the surface atomic layer. For d bands in particular, the absence of nearest-neighbor atoms diminishes the extent of wave-function overlap with the surface atoms. Consequently, the wave-function amplitude for a given bulk state in a d band experiences considerable reduction at the band-edge regions and a concomitant enhancement near the midband. Thus, the normalized spectra for pure d bands would correspond to the solid curve in Fig. 5(b) in which this surface-related band-edge compression is illustrated.

The d bands of the strongly hybridized transition metals under consideration are neither purely d-like nor purely s-p–like. Construction[30] of the band structure of Fig. 3 may be regarded as being compatible with the hybridization among three t_{2g} orbitals (xy form), the two e_g orbitals (x^2-y^2 form), and the s-p–band wave functions. Each of the six subbands is an admixture of the various orbitals whose composition varies widely along each subband dispersion curve. Generally, the spatial extent of the radial part of the d orbitals becomes more confined[30] to the atomic cores in progressing from the bottom to the top of the d-band range (interval from x_3 to x_5 is a useful measure of the d-band width). Consequently, the lower portion of the d bands is regarded as having a bonding character[3] wherein the electron probability is large midway between adjacent bulk atoms. In addition, the Bloch phase factor combines with the orbital symmetries so as to make the t_{2g}- and e_g-band segments bonding (antibonding) at lower (upper) subband edges. Watson *et al.*[32] have argued that charge compression in forming the bulk metal is relaxed at the surface because of the reduced coordination number. Thus, the antibonding states are forced to extend further out of the surface than would be expected on the basis of the free-atom d orbitals. This could explain why the narrower Γ-centered bands are readily observed in the FEED spectra of the platinum-group metals. As more d electrons per atom are encountered in the sequence Ir, Rh, Pt, and Pd, there should be a trend toward greater spatial emergence of the orbitals at the surface for the antibonding segments. Specifically, we may regard an individual subband as having a mixed character in which the central portions are more s-p–like relative to the band-edge portions by reason of the hybridization. Hence, the normalized spectra of these bands would assume the intermediate shape shown in Fig. 5(c) in which a flat, s-p–like portion is sandwiched between two relatively d-like portions. In terms of the local density of states, the competing factors are the probability density versus the density of states in determining the shape of the normalized FEED spectra. Within the midband zone, the degree of d-like admixture could also be reflected in the relative magnitude of the individual subband current contributions to the normalized FEED spectra.

Portions of the electronic bands may involve highly localized constant energy surfaces in k space. According to the band-structure term in Eq. (13), the FEED spectra should demonstrate strongly attenuated contributions from these so-called hole-pocket zones. An illustration of this topologically derived attenuation is sketched in Fig. 5(d) for the upper band-edge region. This might be predicted for the second and third d bands of the platinum-group metals.

To explain some of the various structural shapes contained in the normalized spectra, we recognize the similarities between the above qualitative forms and the results summarized in Fig. 4. The simplest example is represented by the spectra for Pt(100). Decomposition of the curve for Pt(100) begins with the observation that it is composed of three parallel line segments interconnected by relatively abrupt transition segments which correspond with the approximate band-edge locations

of the calculated electronic subbands. If we assume that the subbands are associated with the form of Fig. 5(c) for hybridized bands, then we can perform the decomposition suggested in Fig. 6 by using the additive property, assumed in Eqs. (10) and (11), and the information contained in the band-structure curves of Fig. 3. Beginning from the Γ_{8}^{+} point, we note the overlap of three subbands over the central flat zone. Hence, we are able to extract the composite of the fourth and fifth (Γ-centered) d bands, directly. Since the band structure suggests the continuance of the latter bands well above the Fermi level and the second d band terminates at X_{7}^{+}, the magnitude of the third d band can be obtained by a simple subtraction over the flat zone nearest the Fermi level. Finally, the level of the second d band is established, similarly, over the flat zone below the Γ_{8}^{+} point. Except for differences in their relative magnitudes, the subband contributions are apparently derivable from the simplest model of overlapping free-electron-like bands. The high density of states near band-edge zones appears to be compensated. In view

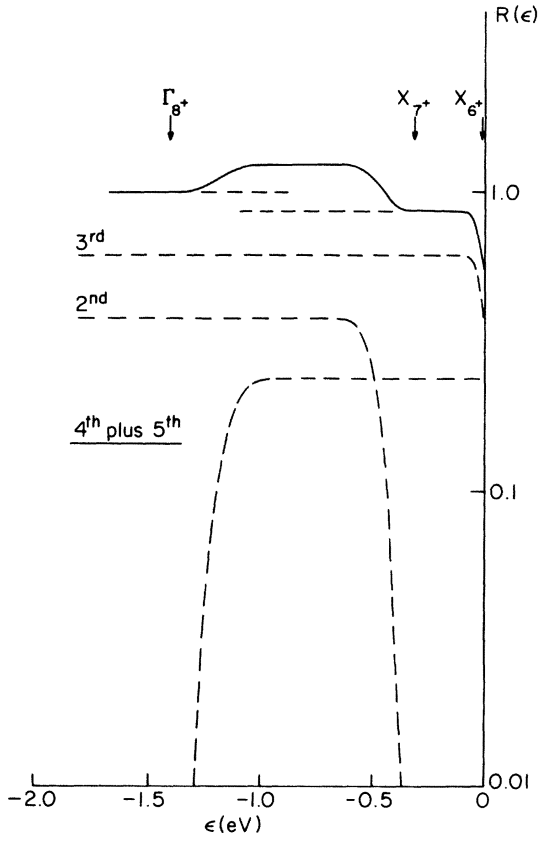

FIG. 6. Spectral decomposition of Pt(100). Dashed curves represent a possible decomposition for the designated d bands.

of the flat central peak, other forms for the constituent curves seem to be less apparent. Remarkably, at the X_{7}^{+} eigenvalue of -0.31 eV, the experimentally-deduced value of -0.35 eV is within the resolution limit of the energy analyzer. Similarly, for the Γ_{8}^{+} point, the calculated value of -1.40 eV is near the experimental value of -1.35 eV. Furthermore, the X_{6}^{+} point seems to occur very near to Fermi level ($\epsilon \cong +0.050$ eV) as indicated by calculation. Thus, these results for Pt(100) apparently represents an instance in which rather good quantitative agreement exists between calculated energy-band structure and FEED spectral structure.

Although the band structure in the $\Delta[100]$ and $\Sigma[110]$ directions differ, they nonetheless terminate at the same eigenvalues. Consequently, these band-edge features should exhibit the same edge locations in the FEED spectra. Indeed, comparison of the normalized curves in Fig. 4 reveals the Γ_{8}^{+}, X_{7}^{+}, and X_{6}^{+} band-edge locations to have nearly identical experimental values for both of these crystallographic directions in platinum. Performing the decompositions as indicated above, we obtain the corresponding d-band contributions illustrated in Fig. 7 for Pt(110). Although the ratio of the second and third d-band contributions remains unchanged at 1.61, we appear to have one-third less contribution from the composite of the Γ-centered bands relative to the Pt(100) result. It is significant that the narrower Γ-centered bands (e_g group) contribute at substantially lower levels relative to the lower-lying t_{2g}-group bands. This suggests a relatively more d-like character for the Γ-centered bands. Note also that there is generally more gradual descent at the band edges in Pt(110). This apparent enhancement of this band-edge compression is consistent with the reduced coordination number of Pt(110) relative to Pt(100) and theoretical arguments[19,21,28,33] in support of this result. The self-consistency is once again demonstrated and extends systematically between related symmetry directions. However, it is not clear why the Γ_{8}^{+} point rather than the $\Gamma_{8}^{+}X_{6}^{+}$ minimum should be the relevant indicator for the band-edge location of the Γ-centered bands of platinum except for the greater d-like character of the fourth d band.

Consideration of the corresponding planes of iridium reveals unexpected current reduction above the onset of the Γ-centered bands ($\epsilon > -1.0$ eV). We cannot postulate on the existence of a band edge below the Fermi level since all four bands have been detected at the Fermi level via de Haas–van Alphen measurements[35] on Ir(100) and Ir(110). However, we might find explanation for this apparent discrepancy by taking note of Andersen's

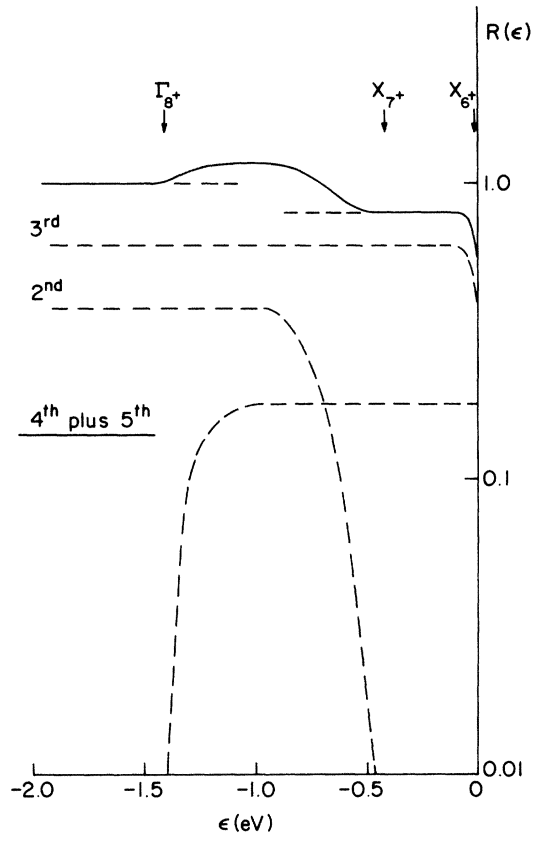

FIG 7. Spectral decomposition of Pt(110). Dashed curves represent a possible decomposition for the designated d bands.

calculated Fermi surfaces for the X_3 and X_4 bands (t_{2g} bands). In both the ⟨100⟩ and ⟨110⟩ directions, these surfaces are closed hole pockets of small cross-sectional area as can be deduced from the Σ' and Z segments of Fig. 3. For the X_3 band, the circular cross section of the Fermi surface intercepts a half-angle of only 4° with respect to the origin. To estimate the FEED spectral current, we may use Fischer's[36] simplification of the band-structure term in Eq. (13) in the effective mass approximation for a spherical energy surface

$$R'(\epsilon) = 1 - e^{-E'/d} , \tag{14}$$

where for an effective-mass ratio r and half-angle θ, we have

$$E' = r(\epsilon - \epsilon_{\min}) \sin^2\theta . \tag{15}$$

Using experimental results from de Haas–van Alphen measurements of Grodski and Dixon[35] in which $r \cong 0.22$, $\theta \cong 4°$, and $E_F \cong 10.8$ eV, we find from Fig. 3 that $R'(\epsilon_F) \cong 0.07$. This is the fractional amount to which the distribution function would be lowered at the Fermi level for the X_3 hole pocket. Our simple calculation is substantially in agreement with the values extracted from the normalized-spectra decompositions of Figs. 8 and 9 for Ir(100) and Ir(110), respectively. It should be noted that this effective-mass approach was employed previously by Cutler and Nagy[37] on W(100). Hence, the second d band apparently experiences upper-band-edge spectral attenuation by reason of the highly directionally confined nature of these hole-pocket zones in the manner indicated by Fig. 5(d). On the other hand, upper-band-edge attenuation does not appear to be as severe for the X_4 (third d-band) hole pocket apparently because of the larger cross-sectional area and effective mass. Actually, we would need the effective-mass values as a function of energy in order to fit the attenuation factor to the herewith approximated contribution for the second and third d bands.

As in the cases for Pt(100) and Pt(110), we are unable to resolve the overlapping Γ-centered band contributions to the spectral curves for Ir(100) and Ir(110). Unlike the results for platinum in which the Γ-centered bands emerge at the Γ_{8+}

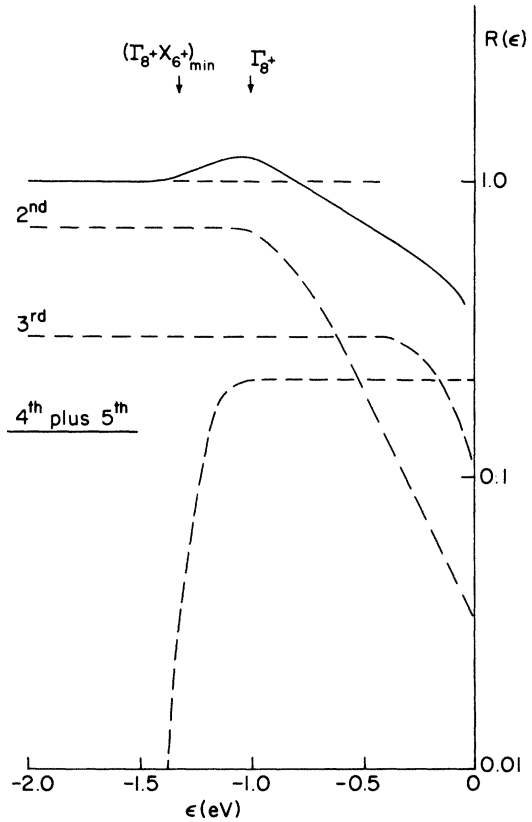

FIG 8. Spectral decomposition of Ir(100). Dashed curves represent a possible decomposition for the designated d bands.

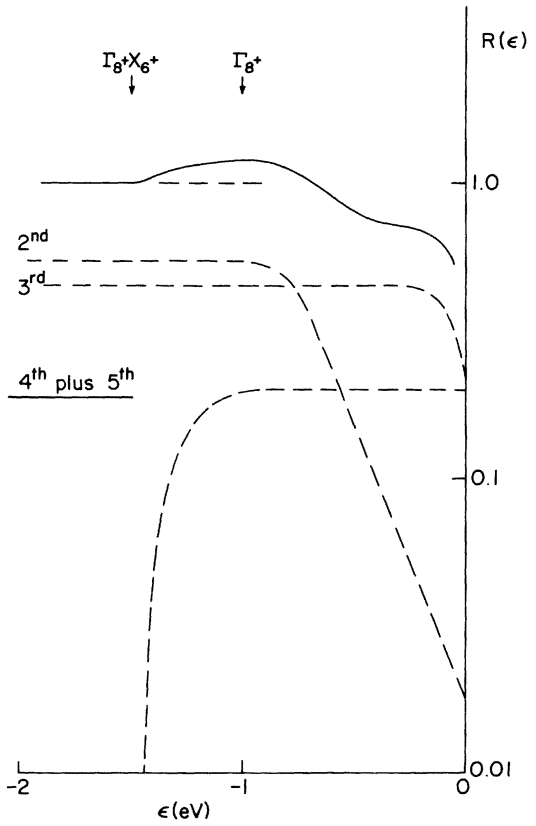

FIG. 9. Spectral decomposition of Ir(110). Dashed curves represent a possible decomposition for the designated d bands.

value, the onset for the structural prominence occurs at the estimated $\Gamma_8^+ X_6^+$ location. Thus, there is some uncertainty regarding the identity of the dominant, but unresolved subband and its precise location. Another difference is the apparent change in the relative contributions of the resolved lower-lying bands in going from iridium to platinum.

If hole-pocket attenuation is to be a valid explanation for the declining, normalized spectral curves of Ir(100) and Ir(110), then it should be equally satisfactory in the interpretation of the corresponding curves for other metals of the platinum group. Application of the above effective-mass method to the second d band of rhodium (X_3) leads to a larger[9] effective mass ($r \cong 0.4$) and a larger angle of inception ($\theta = 8°$) at the Fermi level. The computed attenuation factor of 60% is in reasonable agreement with the estimated experimental value of 70%. For platinum, we unfortunately do not have an experimental or theoretical value of the effective mass for either of the hole-pocket bands since they are located at or just below the Fermi level. But, with one less 6s electron and two additional 5d electrons contributing to this region, we might expect the effective mass to be considerably larger than in the corresponding cases of rhodium and iridium. This is true indeed for palladium which has no 5s electron and nine 4d electrons to contribute to the much flatter d bands. With this additional d-like character, it becomes less obvious how one should proceed with decomposition of the palladium data. Nonetheless, using values[7] of $\theta \cong 4°$, $r \cong 0.62$, $E_F = 7.6$ eV, and $d \cong 0.135$, we calculate a 75% attenuation for the X_3 band at ϵ_F. However, the XW_5, X_3, and X_4 bands have upper-band locations which are very close together, therefore, it is difficult to ascribe a numerical value to the total band attenuation factor (at ϵ_F) which can be compared with the observed attenuation factor of approximately 70%. As noted above the upper band edges (Fig. 3) are comparatively flat. This might explain the rapid attenuation rate near the Fermi level in the Pd(100) spectrum. In brief, use of the effective-mass method for the hole-pocket bands indicates consistent results overall in the interpretation of the enhancement factor curves for all of the four platinum-group metals.

Although decompositions of the individual subband contributions to the normalized FEED spectra is uncertain in some instances, there is useful insight contained in the computed band structure which assists construction of the constituent curves. Since the density of states and effective mass depend upon the reciprocal of the first and second derivative of the dispersion curves, respectively, we are able to deduce the approximate forms for the individual subband contributions and their approximate locations. Normalized spectral curves of rhodium and palladium can be treated in much the same way in which we have considered iridium and platinum. Given the subtle differences in the shapes of the subband dispersion curves, it really should not be surprising that FEED spectra indeed do assume distinctive characteristics for each of the platinum-group metals. An interesting extension of the present work would include similar investigations for binary alloys of the platinum-group metals.

As final examples of spectral decompositions we focus our attention on the curves for Ir(111) and Pt(111). This direction is unique in that we are able to separate the third d band (L_6^-) from the composite of the Γ-centered bands. Consider first the composite band structure for Ir(111) in Fig. 10 along which only the arc segment CD need be estimated (by extending the curve, DE, beyond the obvious knee). The rising portion of the curve AB consists of the band edges of the composite band for which the $\Gamma_8^+ L_6^+$ minimum of the fifth d band

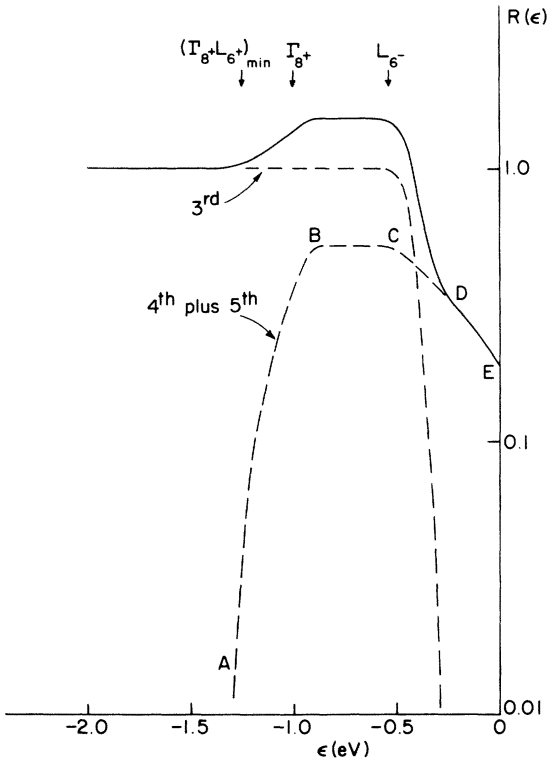

FIG. 10. Spectral decomposition of Ir(111). Dashed curves represent a possible decomposition for the designated *d* bands.

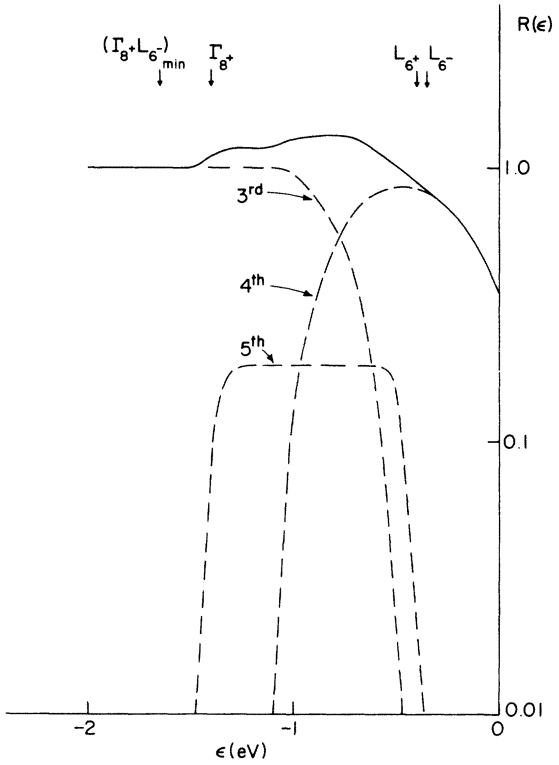

FIG. 11. Spectral decomposition of Pt(111). Dashed curves represent a possible decomposition for the designated *d* bands.

is measured to be −1.30 eV. This compares favorably with Andersen's estimated value of −1.25 eV. Along the flat portion *BC* we observe the same zero slope as for the *s-p*–like third *d*-band contribution; however, the peak of the composite band is only two-thirds the contribution from the L_6^- band. Therefore, the relative contribution to the FEED structure is dependent upon the character of the individual subbands as expected. More significant is the observation that the contributions of the narrower, Γ-centered bands ($L_{4^+5^+}$ and L_6^+) are of the same order of magnitude as the broader *d* band (L_6^-). From the shape of the composite curve, it is apparent that the constituent subband contributions cannot be resolved. Regarding the L_6^- band edge, Andersen's calculated value of −0.54 eV is to be compared with the experimentally derived value of −0.30 eV.

Of the other platinum-group metals, only platinum is calculated to have upper-band-edge locations occurring below the Fermi level in the ⟨111⟩ direction. Experimentally, this prediction appears to be correct for both Rh(111) and Pd(111). However, the normalized spectra for Pt(111) suggest the presence of band edge effects which are not resolvable. Using Fig. 3 as a guide, we find one of many possible three-band decompositions to follow the suggestive pattern portrayed in Fig. 11. To sketch these separated band contributions, we have been forced to lower the L_6^- band edge relative to the $L_{4^+5^+}$ peak which is presumed to be predominant relative to the narrower L_6^+ band. We can not be certain of this more speculative decomposition without some additional experimental information involving perhaps a selective adsorption study. Therefore, the above interpretive decomposition should mitigate concern for the contraction of the anticipated shoulder on the FEED spectrum of Pt(111).

V. LOCAL DENSITY OF STATES

An important feature of the band decompositions performed in the previous section involves the shapes of the constituent curves for the current contributions from the individual subbands. Remarkably, in some instances, FEED spectral contributions of these *d* bands can be described in terms of the spectral shapes associated with *s-p*–like bands. For example, there are three separate, parallel line segments contained in the normalized spectra for Pt(100) and Pt(110). Interpretation of

these curves is straightforward if the spectral shape of the individual subband contributions assumes an s-p-like character. Only the variations in the relative magnitudes of the current contributions seem to identify the d-like nature of these bands in these particular examples. This situation is represented by Eq. (11) in which the directionally weighted, local density of states is summed upon all bands. Similar attempts[2,38] to ascribe band-structure effects to tungsten spectra have been encumbered by uncertainties in the calculated energy-band structure and the nature of the energy bands.

None of the curves associated with the individual band contributions are perfectly flat or rectangular [Fig. 5(a)]. As in the case of Pt(111) and Ir(111), the Γ-centered bands display broadly curved band-edge zones with relatively little extent of central flat zones. In fact, every band edge is characterized by a variety of gracefully descending curves encompassing an energy range greater than a few tenths of an electron volt (considerably larger than the energy analyzer resolution width or other sources of experimental uncertainty). Mention has already been made regarding upper band-edge compression resulting from hole-pocket band-structure effects as evidenced by the second and third d bands. This same attenuation phenomena applies equally well to the lower band edge for the Γ-centered energy surfaces (Duke and Fauchier[38] have pointed out this effect). Although $\theta = \frac{1}{2}\pi$ in Eq. (15), the effective energy ratio E'/d is no longer large compared with unity in Eq. (14). In Fig. 12, we have plotted the normalized energy dependence of the attenuation factor in the free-electron-mass approximation. Typical experimental curves are included in order to illustrate that the band-edge attenuation factor is by itself insufficient to account for the extent of band-edge compression. Insofar as the Γ-centered bands are overlapping and are not reducible to individual subband contributions, it is possible for part of the energy range for this contraction to arise from adjacent band contributions. However, even this staggered overlapping-band hypothesis falls short of the experimentally observed energy range over which this attenuation prevails. From the d-band computations for fcc metals by Haydock and Kelly,[22] the band-edge compression should extend over an energy range of approximately 0.25 eV relative to the bulk values. Their result is consistent with our deduced values of 0.25–0.5 eV from the decompositional results for both upper and lower band-edge attenuation, excluding hole-pocket attenuation effects. Thus, the difference between the ideal and experimentally derived curves in Fig. 12 might be a directionally weighted

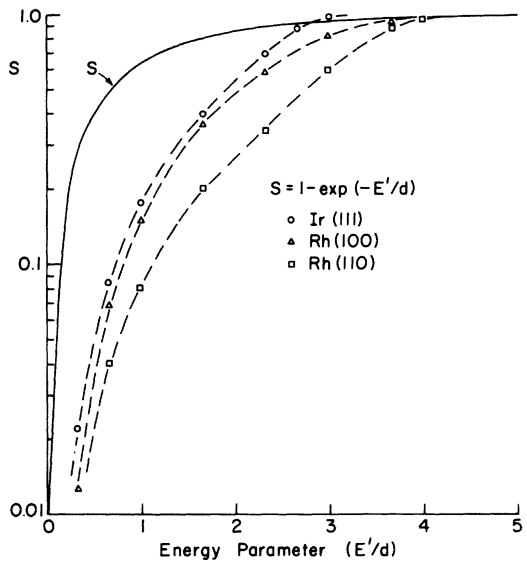

FIG. 12. Band-edge attenuation factor versus normalized energy for Γ-centered band edges. Experimental curves are compared with idealized curve S.

local density of states involving the probability density factor in Eq. (11). Examples of this concept can be viewed in Fig. 4 where the band edges appearing in the curves for the (110) planes are decidedly more gradual than for the symmetry-related (100) planes. These observations are essentially in agreement with the hypothesis[20] that surface atoms of lower coordination number are less coupled to the bulk d bands.

To explain the various structural shapes contained in the normalized FEED spectra, we have introduced a combination of contributions among overlapping subbands of the bulk-band-structure and band-edge attenuation resulting from both energy-surface topology and surface-atom coordination number. Undoubtedly, the variation in the relative mixture of atomic states describing the wave functions also provides another dimension to the observed band-edge compression. Unfortunately, for the transition metals, we do not command quantitative knowledge of the directional, local density of states. Detailed information regarding the wave functions for these strongly hybridized states is generally unavailable. Hence, at present we are unable to make reliable estimates in this regard. In the case of Pd(100), there appears to be an increasing (d-like) current emission from the antibonding region as the X_{7+} edge is approached (Fig. 4). Apparently, the cancellation of the density of states factor is not complete for these less-hybridized d-like bands. Thus, the spectrum for Pd(100) seems to be one

instance in which band-structures topological effects, reduced surface coordination number, and the variable hybridization character along the subband dispersion curves fail to offset the large directional, local density of states associated with subband-edge zones. This interpretation is consistent with the strong antibonding character[32] of the t_{2g} segment in the second d-band for which the spatial extent of the probability density would maximize near the X_{7+}. Thus, our interpretation of the spectral shape is consistent with a more d-like characteristic for this particular hole-pocket band.

At first glance, one might be inclined to interpret the various mounds appearing in Fig. 4 as regions of high density of states since these zones coincide substantially with the low group-velocity portions of the bulk bands of Fig. 3. However, the close agreement between calculated band-edge locations and self-consistent manifestation of s-p-like segments over significant portions of the FEED spectra tend to preclude this alternate view. We can not be entirely certain that the proposed decompositions of Figs. 6–11 represent the most correct deconvolutions of the normalized spectra. However, the self-consistency and reasonableness of these decomposed curves appear to have a basic validity in terms of the overall character of the bulk band structure for these strongly hybridized subbands.

Assuming that we are justified in identifying individual band contributions with the structural content of experimental FEED spectra, we might then expect crystallographic planes in directions differing from the principle planes to provide useful band-structure information. However, the spatial extent over which these planes can be made atomically flat is just marginally adequate for experimental probe-hole measurements, which should be maintained free from undesirable plane-edge current contributions. Since these plane-edge locations can supply current from bulk states other than those having crystal momentum principally normal to the planar surface, experimentally one finds that the FEED spectral details are observed to distort or even to disappear in some instances when the surface planes are not made sufficiently large. Moreover, the actual size of these planes is difficult to estimate from the field-emission screen pattern. Thus, the relatively smaller, open-face planes cannot be anticipated to yield strongly-directional band-structural detail. In addition, symmetry group considerations[2,17] of the compositional mixture of wave functions can seriously alter the tunneling probabilities relative to the predictions[1] based on the WKB model.

In Fig. 13 is shown a collection of normalized FEED spectra for several experimentally-accessible planes of the platinum-group metals (except for palladium). From the shapes of these curves, the relative contributions of the Γ-centered bands are readily apparent. There do not appear to be any important differences among the curves for the ⟨110⟩, ⟨320⟩, and ⟨210⟩ series with the exception of Rh(210). For the latter, we observe attenuation of the Γ-centered bands relative to the lower-lying hole-pocket bands. Explanation for this attenuation can be made in terms of the rapidly decreasing, projected area of the constant energy surface for the third d band as we progress from the ⟨110⟩ to ⟨210⟩ direction (segment Z in Fig. 3). For the cases of Ir(210) and Pt(210), suspected of having planes of insufficient size, edge effects could easily introduce off-normal states from the hole-pocket band since conservation of the transverse component of crystal momentum need not apply at these sites.

These is a trend toward decreasing contribution from the Γ-centered band region in the spectral curves as we pass through the directional sequence: ⟨111⟩, ⟨311⟩, and ⟨211⟩. Until the topology

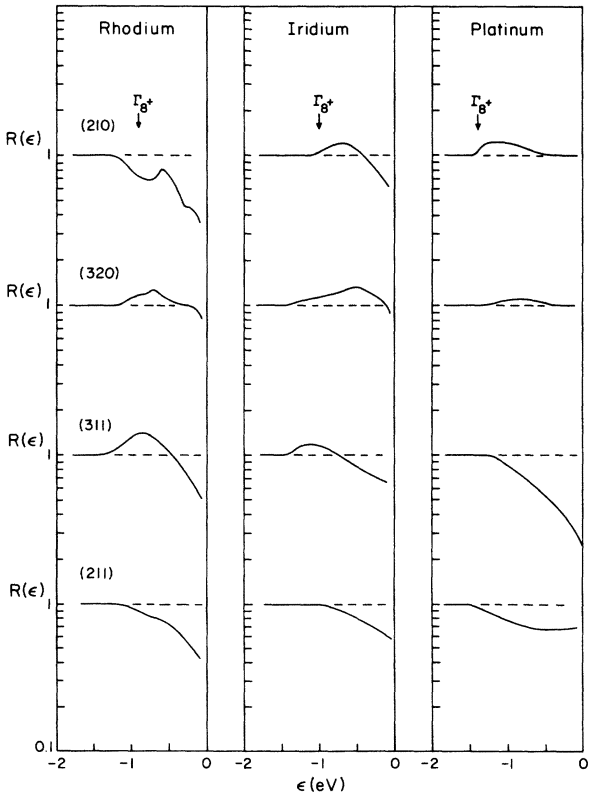

FIG. 13. Enhancement factors for selected clean planes of rhodium, iridium, and platinum.

of the energy surfaces can be described in more detail for these directions, it is difficult to identify with confidence the primary factors influencing this trend. If the Q segment of Fig. 3 is an indication of the topology in the ⟨211⟩ and ⟨311⟩ direction, we then would expect rhodium to experience the least attenuation in the upper-band-edge region of the third d band and platinum to experience the most. It is known from the topology of the Fermi surface[38] that the XW_5 (fourth d band) sheet S an open-hole surface with voids in the ⟨111⟩ direction for platinum and palladium. Thus, attenuation in the data for the (211) and (311) faces should be substantial for this Γ-centered band in platinum near the Fermi level. This might explain some of the observed attenuation in the Γ-band region for the spectral curves for Pt(311) and Pt(211).

Our clean surface results appear to establish the directional character of the band contributions in the FEED spectrum. Furthermore, the band-edge locations are substantially in agreement with theoretical band-structure calculations, once the shapes of the subband contributions are recognized in the normalized spectral data. Other experimental techniques yield complimentary information. The electron spectroscopy for chemical analysis results of Baer[39] have shown the general d-band locations and widths through the bulk density of states with a resolution of 0.5 eV (large compared with our FEED experimental value). Grodski and Dixon's[35] de Haas–van Alphen effect determination of orbits and effective-mass values at the Fermi level have supported Andersen's band-structure computations for iridium. In ultraviolet photoemission investigations, spectra for all four platinum-group metals have been reported for polycrystalline films by Smith[33] and have shown correlation with the band-structural details except for the location of the bands relative to the Fermi level. Our results appear to disagree with Smith's downward adjustment of the band-edge locations relative to the Fermi level except for rhodium in which the Γ-centered bands appear to be ~1.3 eV below Andersen's calculated value. As ultraviolet photoemission results for single-crystal faces become available, it will be interesting to make comparisons with the present work. Unfortunately, only polycrystalline work[34,41-43] is presently reported in the literature for the platinum-group metals. X-ray photoemission spectroscopy[45] and reflectivity[5] measurements have provided complementary joint density of states information.

Recent photoemission studies on Ir(100) by Brodén and Rhodin[44] have indicated a surface resonance at −1.0 eV which appears to attenuate with surface reconstruction. However, no evidence for the surface resonance or reconstruction is suggested in the corresponding FEED spectrum since nitrogen and hydrogen adsorption does not alter the spectral details[19] significantly. Since FEED data are obtained by using field-evaporated tips maintained at liquid-nitrogen temperature, it is possible that spontaneous reconstruction is inhibited at these low temperatures. Unfortunately, momentary heating of the tip to an elevated temperature in order to induce reconstruction creates difficulty with the maintenance of clean surface conditions.

Close inspection of the normalized spectra of Figs. 4 and 13 reveals an overall predominance of t_{2g} bands relative to the e_g (Γ-centered) bands. Since the latter bands are generally narrower and, therefore, can be expected to exhibit more d-like properties, their relative local density of states at the classical turning points are anticipated to be substantially less. However, the remarkable aspect of the spectra is that there is relatively small variation in the relative subband, current contributions among the well-developed, low-index planes. This observation reinforces the hybridized character of these d bands since their FEED spectra seem to reveal an intermediate situation for the s-p or d mix of the tunneling wave functions. Given the predominance of the t_{2g} bands at the metallic surface, their role in the chemisorption process can also be anticipated to be prominent. In Fig. 14, the normalized FEED spectra for the hydrogen and nitrogen covered surfaces (to an equivalent monolayer) are compared with the curves for the principal clean surface planes of rhodium. Notably, manifestations of the Γ-centered bands are conspicuously absent from the curves for the low-index planes. In fact, the spectrum for the adsorbate-covered Rh(111) surface has the shape one would expect for the t_{2g} bands alone. Hence, the wave functions at the modified classical turning points for the adsorption results seem to be composed principally of t_{2g}-band states. Interpretation of this band selectivity will be discussed in a subsequent paper[46] in which is presented generalized adsorption studies of the platinum-group metals. Essentially, the case for rhodium suggests the enhancement of the t_{2g} states at the adlayer with an associated attenuation of the e_g states. Factors such as the wave function symmetries of both the adsorbate and the substrate must be taken into account if the sharp band-edge attenuation in the spectra for the hydrogen-covered Rh(100) and Rh(210) surfaces is to be understood.[19] The chemisorption processes are not limited to k states directed in the surface normal direction; however, normalized

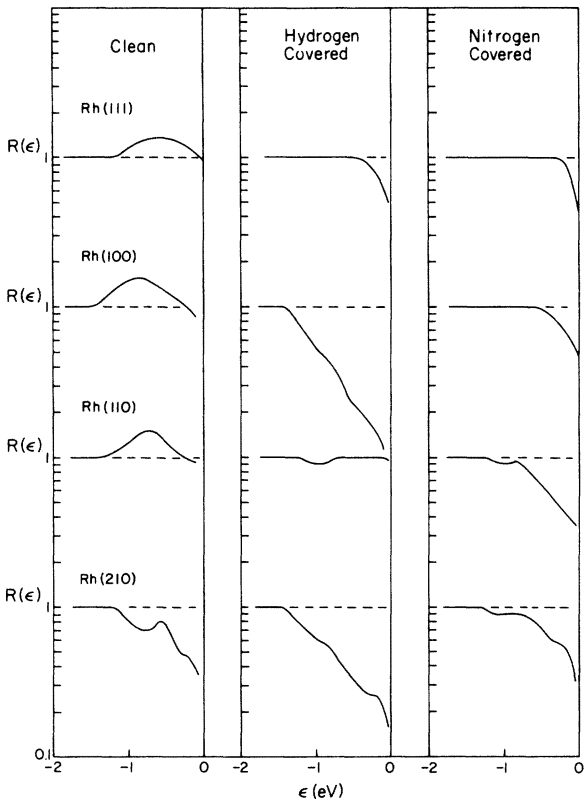

FIG. 14. Enhancement factors for hydrogen and nitrogen absorption on the low-index planes of rhodium.

FEED spectra reflect those states which participate in the surface-normal direction. In the particular case of rhodium, it would appear that the t_{2g} states at normal incidence participate strongly in the chemisorption of hydrogen and nitrogen on the low-index planes.

VI. SUMMARY AND CONCLUSION

Field-emission energy spectra have been measured for probe-hole currents from the principal field-evaporated planes of all four fcc metals of the platinum group. A systematic correlation is observed between subband-edge locations resulting from calculated electronic band structure and experimentally deduced locations based upon a self-consistent interpretation of normalized FEED spectra for the clean atomically flat surfaces of these metals. The band-edge minima for the Γ-centered (e_g) bands near Γ_{8+} appear to be situated within 0.1 eV of the calculated values of O. K. Andersen. Exception is noted for rhodium for which the experimentally determined minima lie at lower levels by a factor of approximately 0.3 eV. Location of the hole-pocket band edge (X_{7+}) is in close agreement with calculated eigenvalues ($\epsilon = -0.136$, -0.31, and -0.31 eV, respectively) for Pd(100), Pt(100), and Pt(110). Similarly, the X_{6+} eigenvalue ($\epsilon = -0.05$ eV) coincides with the pronounced, spectral attenuation effects for Pt(100) and Pt(110). Finally, the upper-edge location of a spectral prominence in the data for Ir(111) is situated near the computed value for $L_{6-}(\epsilon = -0.54$ eV).

Using the electronic band structure as a guide, we have performed some suggested decompositions of the normalized FEED spectra into contributions among the overlapping subbands. The starting point in these reductions is an assumption regarding the s-p-like character of the strongly hybridized, t_{2g} bands over their middle energy range. Perhaps the most interesting aspect of the decomposed curves is the shape of the individual subband current contributions. With the exception of Pd(100), the normalized spectral curves for the individual bands are interpreted to be remarkably free from the anticipated high density-of-states peaks near the subband edge locations. Causes for this band-edge attenuation are ascribed to a combination of contributing effects which include (i) the energy surface topology, (ii) the hybridized nature of the subbands and energy surfaces, (iii) band-edge compression resulting from reduced coordination number of surface atoms, and (iv) the presumption that a directionally weighted, local density of states is measured at the classical turning points. For the band-edge regions of these hybridized bands, the tunneling probability would be reduced sharply because of the increased thickness of the surface potential barrier for the pure d-like states. Overall, the uniqueness of the spectral curves for each surface plane of the emitters strongly suggests the directional character of the local density of states, sampled in FEED spectra. The t_{2g} bands seem to predominate in the normalized spectral curves for the low-index planes.

Adsorption of saturation layers of hydrogen and nitrogen on the (100), (110), (210), and (111) faces of rhodium provide significantly altered normalized spectra. These spectral differences are interpreted in terms of enhanced current contributions among band segments of the t_{2g} symmetry group relative to the e_g symmetry group.

ACKNOWLEDGMENTS

The authors are grateful for the opportunity of discussing the theoretical implications of field-tunneling spectra with Paul Soven, University of Pennsylvania. We also thank Robert Billington for helpful discussions and for experimental assistance. Research support by ARPA through the Cornell Materials Science Center and through NSF Grant No. DNR 71-01769 A02 is also gratefully acknowledged.

*Work supported by ARPA through the Cornell Materials Science Center and through NSF Grant No. DMR 71-01769 A02.

†Present affiliation: Raytheon Co., Waltham, Mass.
‡Address inquiries to this author.

[1]D. R. Penn and E. W. Plummer, Phys. Rev. B 9, 1216 (1974).
[2]B. Politzer and P. H. Cutler, Mat. Res. Bull. 5, 703 (1970); Phys. Rev. Lett. 28, 1330 (1972).
[3]H. D. Hagstrom and G. E. Becker, Phys. Rev. 159, 572 (1967).
[4]A. Liebsch, Phys. Rev. Lett. 32, 1203 (1974).
[5]J. H. Weaver, Phys. Rev. B 11, 1416 (1975).
[6]L. W. Swanson and A. E. Bell, *Advances in Electronics and Electron Physics* (Academic, New York, 1973), Vol. 31.
[7]J. W. Gadzuk and E. W. Plummer, Rev. Mod. Phys. 45, No. 3 (1973).
[8]N. J. Dionne and T. N. Rhodin, Phys. Rev. Lett. 32, 1311 (1974).
[9]O. K. Andersen, Phys. Rev. B 2, 883 (1970); Ph.D. thesis (Technical University of Denmark, 1969) (unpublished).
[10]R. D. B. Whitcutt and B. H. Blott, Phys. Rev. Lett. 23, 639 (1969).
[11]L. W. Swanson and L. C. Crouser, Phys. Rev. Lett. 16, 389 (1966); 19, 1174 (1967); Phys. Rev. 163, 622 (1969).
[12]M. Campagna and T. Utsumi, AIP Conf. Proc. 24, 399 (1974).
[13]E. W. Plummer and J. W. Gadzuk, Phys. Rev. Lett. 25, 1493 (1970).
[14]C. Lee and R. Gomer, J. Chem. Phys. 54, 3349 (1971).
[15]C. B. Duke and J. Fauchier, Surf. Sci. 32, 175 (1972).
[16]J. W. Gadzuk, Phys. Rev. 182, 416 (1969).
[17]N. Nicolau and A. Modinos, Phys. Rev. B 11, 3687 (1975).
[18]T. V. Vorburger, D. Penn, and E. W. Plummer, Surf. Sci. 48, 417 (1975).
[19]N. J. Dionne, Ph.D. thesis (Cornell University, 1975) (unpublished).
[20]V. Heine, Proc. R. Soc. Lond. A 331, 307 (1972); Proc. Phys. Soc. Lond. 81, 300 (1963).
[21]J. Friedel, Adv. Phys. 3, 446 (1954).
[22]R. Haydock and M. J. Kelly, Surf. Sci. 38, 139 (1973).
[23]D. Kalkstein and P. Soven, Surf. Sci. 26, 85 (1971).
[24]F. I. Itskovich, Soc. Phys.-JETP 23, 945 (1966); 25, 1143 (1967).
[25]R. Stratton, Phys. Rev. 135, A794 (1964).
[26]J. Politzer and T. E. Feuchtwang, Phys. Rev. B 3, 597 (1971).
[27]J. Appelbaum and W. F. Brinkman, Phys. Rev. 186, 464 (1969).
[28]R. D. Young, Phys. Rev. 113, 110 (1957).
[29]H. D. Hagstrum and G. E. Becker, J. Chem. Phys. 54, 1015 (1971).
[30]N. F. Mott, Adv. Phys. 13, 325 (1964).
[31]J. H. Wood, Phys. Rev. 117, 714 (1960).
[32]P. Fulde, A. Lüther, and R. E. Watson, Phys. Rev. B 8, 440 (1973); and L. Hodges, R. E. Watson, and E. Ehrenreich, *ibid.* 5, 3953 (1972).
[34]N. V. Smith, Phys. Rev. B 9, 1341 (1974); N. V. Smith, G. K. Wertheim, and S. Hüfner, *ibid.* 10, 3197 (1974).
[35]J. J. Grodski and A. E. Dixon, Phys. Rev. B 6, 1198 (1972).
[36]R. Fischer, Phys. Status Solidi 2, 1088 (1962).
[37]D. Nagy and P. H. Cutler, Phys. Rev. 186, 651 (1969).
[38]E. W. Plummer (University of Pennsylvania, private communication).
[39]J. B. Ketterson, F. M. Mueller, and L. R. Windmiller, Phys. Rev. 186, 656 (1969).
[40]Y. Baer, P. F. Heden, J. Hedman, M. Klasson, C. Nordling, and K. Siegbahn, Phys. Scr. 1, 55 (1970).
[41]S. F. Lin, D. T. Pierce, and W. E. Spicer, Phys. Rev. B 4, 326 (1971).
[42]J. F. Januk, D. E. Eastman, and A. R. Williams, Solid State Commun. 8, 271 (1970).
[43]D. T. Pierce and W. E. Spicer, Phys. Rev. B 5, 2125 (1972).
[44]G. Brodén and T. Rhodin, Solid State Commun. 18, 105 (1976).
[45]S. Kowalczyk, L. Ley, R. Pollak, and D. A. Shirley, Phys. Rev. Lett. 29, 274 (1972); 41, 455 (1972).
[46]R. Billington, N. J. Dionne, and T. N. Rhodin, Surf. Sci. (to be published).

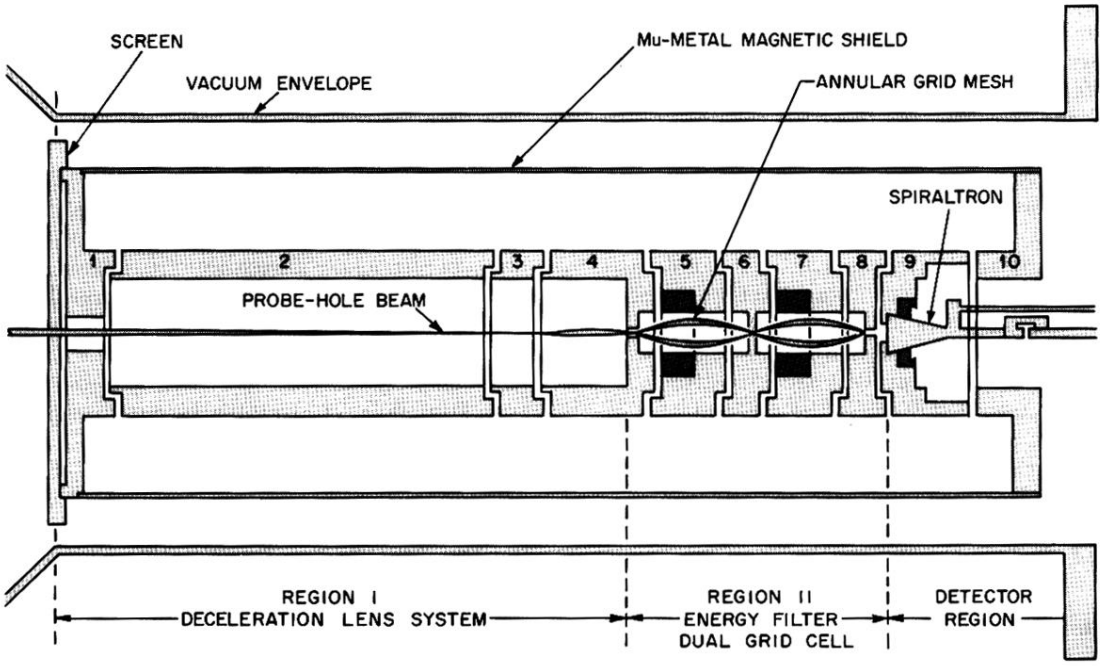

FIG. 1. Grid-cell energy analyzer.